Rapid printing of metal nanostructures through projection-based two-photon reduction

Jungho Choi, Harnjoo Kim, Sourabh K. Saha*

G.W. Woodruff School of Mechanical Engineering, Georgia Institute of Technology, Atlanta 30332, GA, USA

*Corresponding author: <u>ssaha8@gatech.edu</u>

Abstract

Two-photon reduction (TPR) is a laser-based technique that can print nanostructures through localized photoreduction of metal ions into nanoparticles. However, its throughput is limited by the point-by-point printing mechanism. Here, we present a projection based TPR technique to print arbitrarily complex 2D patterns at once. Our technique scales up TPR through projection of patterned femtosecond light sheets. We demonstrate printing of silver features as small as 300 nm and achieve an areal printing rate up to 10 mm²/min, which is 30 times faster than past demonstrations of TPR. Our technique can therefore significantly advance the scalability of manufacturing metallic nanostructures.

Keywords: Direct writing, Multi-photon printing, Femtosecond projection, Laser processing, Silver printing

1. Introduction

Metallic structures with in-plane dimensions on the 100 nm length scale are desirable for a variety of applications such as flexible electronics [1], plasmonics-based chemical and bio-sensing [2, 3], photonics [4, 5], quantum-enabled devices [6, 7], micro-robotics [8], and micro-electro-mechanical-systems (MEMS) [9]. Currently, manufacturing of these nanostructures is limited by the need for foundry-based micro-fabrication and expensive physical masks. These constraints make it challenging to achieve affordable manufacturing at low production volumes. Laser-based direct writing techniques provide a promising alternate approach for maskless fabrication of nanostructures [10, 11]. Two-photon reduction (TPR) is one such laser-based technique that can generate nanostructures through localized photoreduction of metal ions into metal nanoparticles [12-15]. It exhibits minimal material wastage because metal nanoparticles are selectively generated only in the illuminated region. However, the throughput of TPR is limited by its serial point-by-point printing mechanism. Here, we have overcome this limitation by massively parallelizing TPR while maintaining its fine sub-diffraction resolution.

TPR relies on nonlinear two-photon absorption to achieve sub-diffraction nanoscale printing [13, 16]. Fine resolution on the 200 nm scale can be achieved in TPR because appreciable light absorption occurs only in a small fraction of the focal volume wherein the optical intensity is very high (~1 TW/cm²) [12, 13]. Such high intensities can be achieved through focusing of femtosecond (fs) light [17]. Despite its fine resolution, TPR has remained a niche technique with limited adoption beyond research laboratories because of its low printing rate. The printing rates for serial scanning TPR are ~20 μ m²/s with typical linear scanning speeds of 5–50 μ m/s [13, 14, 16, 18-23]. Past attempts at parallelization have further increased the rate by only 2-3 times and those approaches could only fabricate a limited set of geometries [24, 25]. We have previously demonstrated how one may increase the scanning speed of serial TPR by a thousand times (to 10 mm/s) through optimization of the ink composition [26]. However, further scale-up of the serial scanning mechanism is challenging. Here, we have overcome the scale-up challenge by parallelizing the illumination mechanism which enables one to print arbitrarily complex 2D patterns as large as 130 μ m × 130 μ m in 100 ms time scales.

Our projection-TPR (P-TPR) technique is based on the projection of patterned femtosecond 2D light sheets. The light sheet consists of hundreds of thousands of closely spaced focal spots that can be individually switched on and off. The projection mechanism is similar to the one in our past demonstration of nanoscale 3D printing of polymeric materials [27]. Here, we present (i) the modification of the projection-based printing technique to enable metal printing with aqueous inks and (ii) manufacturing performance characterization of silver printing using the P-TPR process. The manufacturing capability presented here can be applied widely to print a variety of noble metal nanostructures via photoreduction.

2. Material and methods

We have used a custom-built printer to implement P-TPR. A schematic of the printer is illustrated in Fig. 1. Printing was performed with a femtosecond laser amplifier (Spectra-Physics Solstice Ace). It has a center wavelength of 800 nm, a repetition rate of 5 kHz, a pulse duration shorter than 35 fs, and an average optical power more than 5 W. The laser beam was patterned by reflecting it off a digital micromirror device (DMD) which acts as a digital mask. The beam can be patterned into arbitrary shapes by loading digital bitmap images onto the DMD. The individual pixels in the DMD turn 'on' or 'off' based on the bitmap pixel value corresponding to one or zero, respectively. We have used the commercially available DLP Lightcrafter 6500 system to set up and control the DMD. The 'on' beams from all bright pixels of the DMD were collected using a collimated lens and then focused into the aqueous ink solution using an objective lens. The two lenses were arranged in a 4f-like arrangement which ensures temporal focusing of the fs light, i.e.,

it ensures that the intensity of light is highest at the focal plane and the intensity fades away with increasing distance from the focal plane. Details of the temporal focusing mechanism are available elsewhere [27].

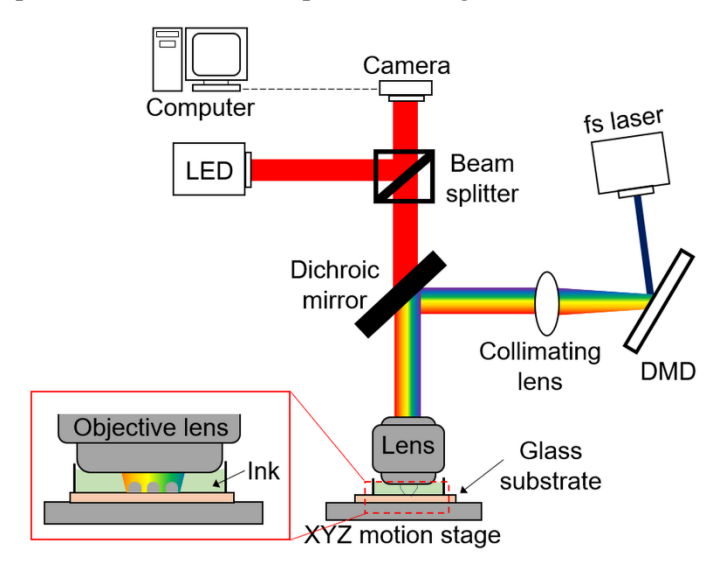


Figure 1: Schematic of the custom-built P-TPR printer.

We performed printing with a custom ink blend that was synthesized by mixing commercially available chemicals. The ink was formulated based on our previous work on serial TPR [26]. The ink comprises a mixture of silver nitrate, ammonium hydroxide, trisodium citrate, 7-diethylamino-3-thenoylthenoylcoumarin (DETC), ethanol, and deionized distilled water. Silver nitrate and ammonium hydroxide were mixed in a stoichiometric ratio to generate diamminesilver(I) ions ([Ag(NH3)2]⁺) which is the source of the silver ions in the ink. Trisodium citrate acts as a reducing agent whereas DETC acts as the photosensitizer. The molar concentration of diamminesilver(I) ions was 0.4M, the concentration of trisodium citrate was 0.13M, and the concentration of DETC was 0.1% by weight.

We used a multi-immersion objective lens (Zeiss plan neofluar 40× 0.9 NA) which was set to the water immersion mode to minimize spherical aberrations in the aqueous ink. The objective lens was dipped directly into the ink while the ink was supported on top of a glass substrate. The focal plane was positioned to lie at the ink-substrate interface so that silver nanostructures could be printed on top of the glass substrate. After printing, the glass substrates were developed by first dipping them into deionized distilled water for 10 minutes and then dipping them into isopropanol for 10 minutes. When printed on the bare glass substrates, discontinuities were observed in fine sub-micrometer line features due to the partial detachment of silver from glass during development. Therefore, during printing of line features, this effect was mitigated by chemically modifying the surface of the glass substrates to improve the adhesion of silver. Glass substrates were treated before printing by dipping them into 0.1M aqueous solution of diallyldimethylammonium chloride for an hour based on protocol available in the literature [28].

3. Results and discussion

Representative nanostructures that were printed using P-TPR are shown in Fig. 2. Each sub-part of the figure shows the structures that were printed simultaneously using a single projection with light exposures lasting up to 500 ms. The printed areas are those that appear bright in the scanning electron microscopy (SEM) images. Presence of silver in the printed areas was confirmed through energy-dispersive X-ray spectroscopy (EDS). It is noteworthy that carbon from the ink was not detected at any appreciable level in the printed regions. This is likely due to the effects of the high-intensity femtosecond laser illumination

which leads to removal of the carbon. In addition to silver (at 34%), the EDS data showed a significant proportion of silicon (at 25%) and oxygen (at 34%) in the printed regions. We suspect that the silicon and oxygen from the underlying glass substrate were being detected during EDS. To verify this hypothesis, we performed atomic force microscopy (AFM) and measured the height of the printed nanostructures in the GT logo. The average height was measured to be 92 nm with a root mean square (RMS) surface roughness of 18 nm. This supports our hypothesis that the silicon and oxygen detected during EDS are from the glass substrate as the characterization volume of the EDS is on the 1 µm length scale. The EDS and the AFM data are available in the supplementary materials.

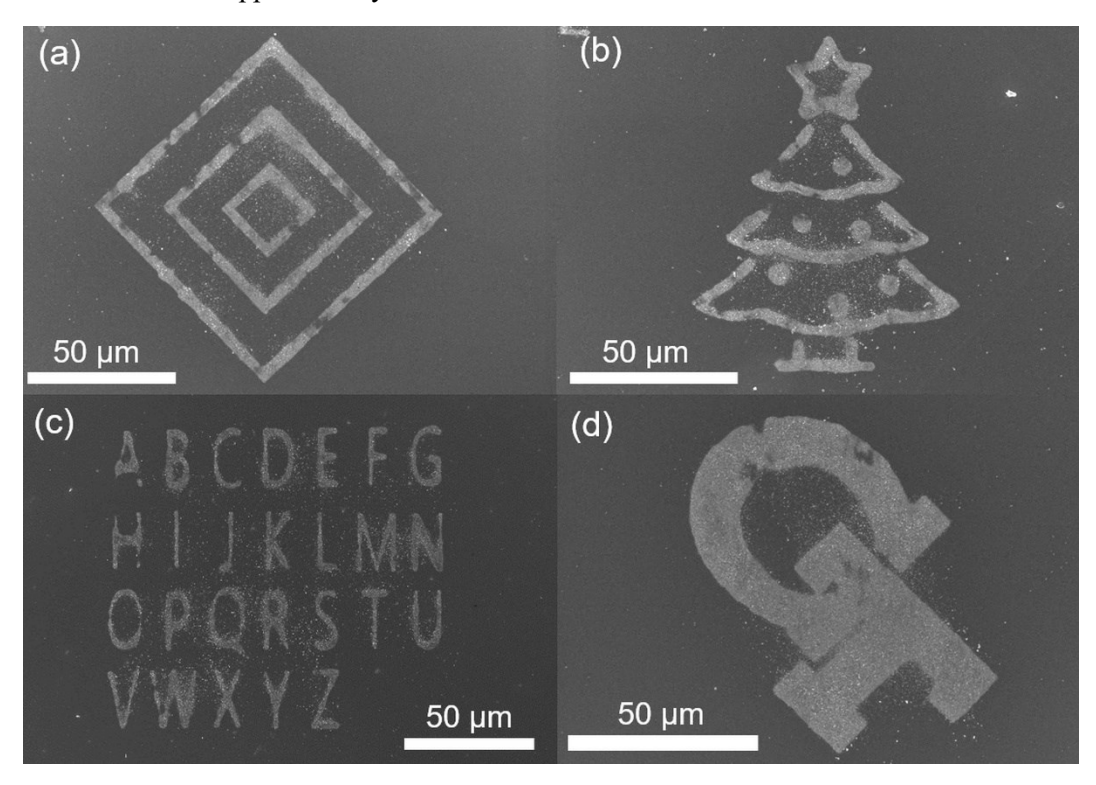


Figure 2: Scanning electron micrographs of the printed silver nanostructures. Within each sub-part image (a)-(d), all features were printed at once by projecting a single bitmap image.

We performed additional experiments to quantify the printing rate and the resolution of line printing, i.e., the width of the finest printable line. The results of these studies are summarized in Fig. 3. Arrays of lines were printed under various optical powers (70 – 128 nW/pixel) and exposures (80 – 600 ms). The lower limit for exposure was determined from the minimum exposure required for printing whereas the upper limit was determined from the exposure at which large bubbles were formed due to excessive heating. The time-averaged power of 128 nW/pixel corresponds to a peak intensity of 2.5 TW/cm² and when exposed for 100 ms results in a fluence of 55 J/cm² (power to intensity and fluence conversions are available in the supplementary materials). This peak intensity is comparable to that observed in the two-photon polymerization technique [17, 29]. SEM images of representative printed arrays are shown in Fig. 4. The widths were measured for the rightmost line at the top section of each image and the standard deviation was obtained from the variations in the linewidth along the length. It was observed that the width of the printed lines increased with an increase in the optical power and the exposure; this is consistent with the expected behavior. As the fluence increases with an increase in the power and exposure time, it can be concluded from Fig. 3 that the width increases with an increase in the fluence.

Each line was 6-pixel wide in the projected image and the array period was 30 pixels. The projection system demagnified each pixel to a size of 152 nm at the focal plane; therefore, the nominal width of the projected lines was 912 nm. The diameter of the diffraction-limited spot that can be achieved by focusing the laser beam of 800 nm wavelength (λ) into a single focal spot is 1084 nm (=1.22 λ /NA). It is evident from Fig. 3 that the widths of the lines printed under several operating conditions are finer than both the nominal projected linewidth and the diffraction-limited spot size. The width of the thinnest line in Fig. 3 is 308 nm. Thus, fine sub-diffraction printing can be achieved with P-TPR.

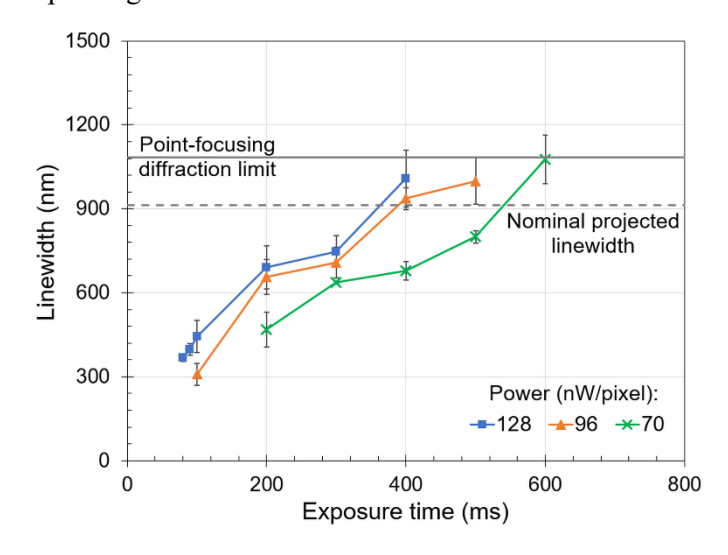


Figure 3: Effect of the exposure time on the linewidth of the printed features under different incident optical powers. All projected lines were 6-pixel wide with each pixel being 152 nm wide.

Although a clear trend was observed for the dependence of linewidths on process parameters, a clear trend for the heights of the lines could not be identified (height data available in the supplementary material). When the power is held constant, the height increases with the exposure time but the height does not seem to increase with an increase in the power when the exposure is held constant. The heights of the lines were in the range of 20-45 nm and on the same scale as the size of the individual nanoparticles. In contrast, multiple nanoparticles aggregated together along the width dimension to form the lines. We suspect that the height is predominantly determined by the nanoparticle nucleation growth dynamics whereas the width is predominantly determined by the size of the light spot. Accurately deciphering the underlying mechanisms will require additional work. Nevertheless, our work demonstrates that sub-micrometer metallic lines can be printed with deterministic control of widths using the P-TPR technique.

The high-throughput of P-TPR originates from its area processing approach wherein areas as large as $130 \, \mu m \times 130 \, \mu m$ can be printed at once within 100-500 ms. This results in an areal printing rate of $2-10 \, mm^2/min$. When compared with past demonstrations of serial and parallel TPR by other researchers [20, 24], the rate of P-TPR is up to 3,000 times higher. When compared with our own past work on serial TPR [26], the rate of P-TPR is up to 30 times higher (rate evaluations available in the supplementary materials). Thus, P-TPR is capable of high-throughput printing of metallic nanostructures without sacrificing the nanoscale sub-diffraction resolution.

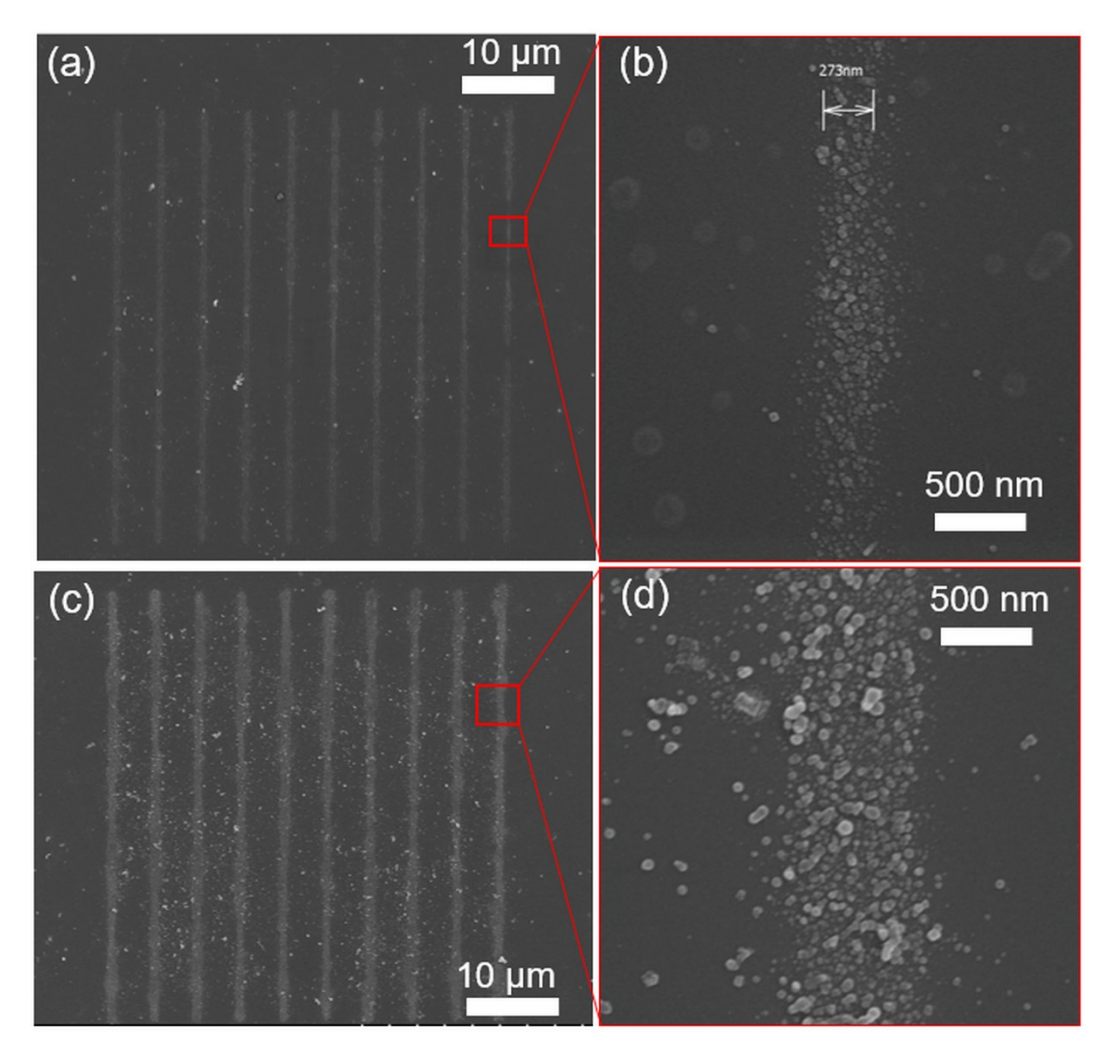


Figure 4: Scanning electron micrographs of arrays of line features printed with 6-pixel wide line projections and at 96 nW/pixel power. (a) and (b) Upon exposure for 100 ms. (c) and (d) Upon exposure for 300 ms.

4. Conclusions

Here, we have demonstrated that the femtosecond laser-based P-TPR technique can rapidly print silver nanostructures through localized photoreduction of an aqueous ionic solution of silver ions. Our technique implements a projection-based parallelization mechanism to print arbitrarily complex patterns. Features with in-plane dimensions as small as 300 nm can be printed within 100 ms time scales and over areas as large as $130 \, \mu m \times 130 \, \mu m$. Our technique increases the rate of printing in TPR by up to 3,000 times relative to the past work of other researchers and by up to 30 times relative to our own past work. It can therefore significantly advance the scalability of light-directed metal nanomanufacturing for a wide range of applications including electronics, photonics, sensing, optical metamaterials, and MEMS.

Acknowledgements

This work was partly supported by the National Science Foundation (NSF) CAREER award 2045147. Imaging was performed at the Georgia Tech Institute for Electronics and Nanotechnology, a member of the National Nanotechnology Coordinated Infrastructure (NNCI), which is supported by NSF (ECCS-2025462).

References

- [1] Shrivas K, Ghosale A, Bajpai PK, Kant T, Dewangan K, Shankar R. Advances in flexible electronics and electrochemical sensors using conducting nanomaterials: A review. Microchemical Journal. 2020;156:104944.
- [2] Tokel O, Inci F, Demirci U. Advances in plasmonic technologies for point of care applications. Chemical reviews. 2014;114:5728-52.
- [3] Singh P. SPR biosensors: historical perspectives and current challenges. Sensors and actuators B: Chemical, 2016;229:110-30.
- [4] Lindquist NC, Nagpal P, McPeak KM, Norris DJ, Oh S-H. Engineering metallic nanostructures for plasmonics and nanophotonics. Reports on Progress in Physics. 2012;75:036501.
- [5] Wang G, Liu T, Chao J, Jin H, Liu J, Zhang H, et al. Recent Advances and Challenges in Ultrafast Photonics Enabled by Metal Nanomaterials. Advanced Optical Materials. 2022:2200443.
- [6] Bogdanov SI, Makarova OA, Xu X, Martin ZO, Lagutchev AS, Olinde M, et al. Ultrafast quantum photonics enabled by coupling plasmonic nanocavities to strongly radiative antennas. Optica. 2020;7:463-9.
- [7] Wei H, Yan X, Niu Y, Li Q, Jia Z, Xu H. Plasmon–exciton interactions: spontaneous emission and strong coupling. Advanced Functional Materials. 2021;31:2100889.
- [8] Kiziroglou ME, Temelkuran B, Yeatman EM, Yang G-Z. Micro motion amplification—a review. IEEE Access. 2020;8:64037-55.
- [9] Tilli M, Paulasto-Krockel M, Petzold M, Theuss H, Motooka T, Lindroos V. Handbook of silicon based MEMS materials and technologies: Elsevier, 2020.
- [10] Ma Z-C, Zhang Y-L, Han B, Chen Q-D, Sun H-B. Femtosecond-Laser Direct Writing of Metallic Micro/Nanostructures: From Fabrication Strategies to Future Applications. Small Methods. 2018;2:1700413.
- [11] Sakamoto M, Fujistuka M, Majima T. Light as a construction tool of metal nanoparticles: Synthesis and mechanism. Journal of Photochemistry and Photobiology C: Photochemistry Reviews. 2009;10:33-56.
- [12] Tabrizi S, Cao Y, Lin H, Jia B. Two-photon reduction: a cost-effective method for fabrication of functional metallic nanostructures. SCIENCE CHINA Physics, Mechanics & Astronomy. 2017;60:034201.
- [13] Ishikawa A, Tanaka T, Kawata S. Improvement in the reduction of silver ions in aqueous solution using two-photon sensitive dye. Applied physics letters. 2006;89:113102.
- [14] Tanaka T, Ishikawa A, Kawata S. Two-photon-induced reduction of metal ions for fabricating three-dimensional electrically conductive metallic microstructure. Applied Physics Letters. 2006;88:081107.
- [15] Palmer T, Waller EH, Andrä H, Steiner K, von Freymann G. Simulation Model for Direct Laser Writing of Metallic Microstructures Composed of Silver Nanoparticles. ACS Applied Nano Materials. 2021.

- [16] Cao Y-Y, Takeyasu N, Tanaka T, Duan X-M, Kawata S. 3D Metallic Nanostructure Fabrication by Surfactant-Assisted Multiphoton-Induced Reduction. Small. 2009;5:1144-8.
- [17] Baldacchini T. Three-dimensional microfabrication using two-photon polymerization: fundamentals, technology, and applications: William Andrew, 2015.
- [18] LaFratta CN, Lim D, O'Malley K, Baldacchini T, Fourkas JT. Direct laser patterning of conductive wires on three-dimensional polymeric microstructures. Chemistry of materials. 2006;18:2038-42.
- [19] Tabrizi S, Cao Y, Cumming BP, Jia B, Gu M. Functional optical plasmonic resonators fabricated via highly photosensitive direct laser reduction. Advanced Optical Materials. 2016;4:529-33.
- [20] Ishikawa A, Tanaka T. Two-photon fabrication of three-dimensional metallic nanostructures for plasmonic metamaterials. Journal of Laser Micro Nanoengineering. 2012;7:11.
- [21] Lu W-E, Zhang Y-L, Zheng M-L, Jia Y-P, Liu J, Dong X-Z, et al. Femtosecond direct laser writing of gold nanostructures by ionic liquid assisted multiphoton photoreduction. Optical Materials Express. 2013;3:1660-73.
- [22] He G-C, Zheng M-L, Dong X-Z, Jin F, Liu J, Duan X-M, et al. The conductive silver nanowires fabricated by two-beam laser direct writing on the flexible sheet. Scientific reports. 2017;7:1-8.
- [23] Barton P, Mukherjee S, Prabha J, Boudouris BW, Pan L, Xu X. Fabrication of silver nanostructures using femtosecond laser-induced photoreduction. Nanotechnology. 2017;28:505302.
- [24] Qian D, Yang L, Zhang Y, Xin C, Hu Z, Hu K, et al. Flexible and rapid fabrication of silver microheaters with spatial-modulated multifoci by femtosecond laser multiphoton reduction. Optics letters. 2018;43:5335-8.
- [25] Liu L, Yang D, Wan W, Yang H, Gong Q, Li YJN. Fast fabrication of silver helical metamaterial with single-exposure femtosecond laser photoreduction. 2019;8:1087-93.
- [26] Saha SK, Au B, Oakdale JS. High-Speed Direct Laser Writing of Silver Nanostructures via Two-Photon Reduction. Advanced Engineering Materials. 2019;21:1900583.
- [27] Saha SK, Wang D, Nguyen VH, Chang Y, Oakdale JS, Chen S-C. Scalable submicrometer additive manufacturing. Science. 2019;366:105-9.
- [28] Wu D, Yao B, Wu S, Hingorani H, Cui Q, Hua M, et al. Room-Temperature Annealing-Free Gold Printing via Anion-Assisted Photochemical Deposition. Advanced Materials. 2022;34:2201772.
- [29] Oakdale JS, Smith RF, Forien JB, Smith WL, Ali SJ, Bayu Aji LB, et al. Direct laser writing of low-density interdigitated foams for plasma drive shaping. Advanced Functional Materials. 2017;27:1702425.

Supplementary Materials for

Rapid printing of metal nanostructures through projection-based two-photon reduction

Jungho Choi, Harnjoo Kim, Sourabh K. Saha*

G.W. Woodruff School of Mechanical Engineering, Georgia Institute of Technology, Atlanta 30332, GA, USA

*Corresponding author: ssaha8@gatech.edu

This PDF file includes:

Supplementary Text Figures S1 to S4 Tables S1 to S3

S1. Energy-dispersive X-ray spectroscopy (EDS) data

The printed GT logo structure that was used to perform the EDS analysis is shown in Fig. S1. EDS was performed on the Hitachi SU8230 scanning electron microscope (SEM) which is equipped with an energy-dispersive X-ray spectroscope. The region over which the measurements were taken has been marked with a rectangular box. The composition of the investigated region is listed in Table S1.

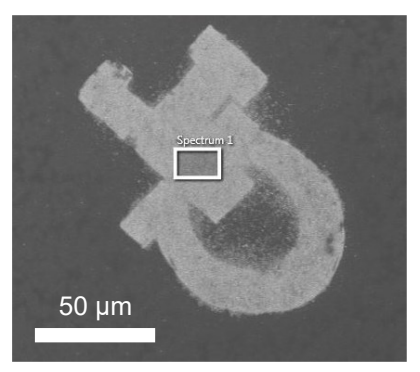


Figure S1: SEM image of the GT logo highlighting the central region over which EDS was performed.

Table S1: Composition of the printed region as obtained from EDS analysis

#	Element	Weight %	Standard deviation (%)
1	О	34.2	3.4
2	Ag	33.8	6.2
3	Si	25.4	2.6
4	Na	6.7	0.9

S2. SEM image of lines at finest resolution of 300 nm

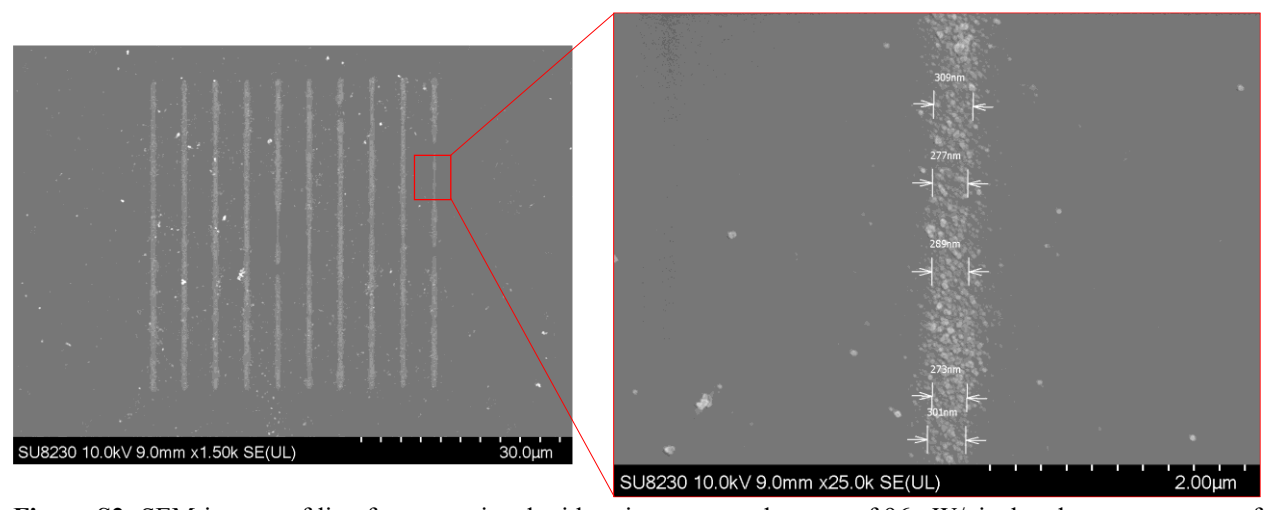


Figure S2: SEM images of line features printed with a time-averaged power of 96 nW/pixel and at an exposure of 100 ms.

S3. Atomic force microscopy (AFM) data

An AFM image of the GT logo was captured using a Bruker ICON scanning probe microscope in the tapping mode. The image is shown in Fig. S3. The region over which the average height and the root mean

square (RMS) surface roughness (S_q) were evaluated is marked on the image using a rectangular box. The measured average height was 92 nm and the S_q was 18 nm.

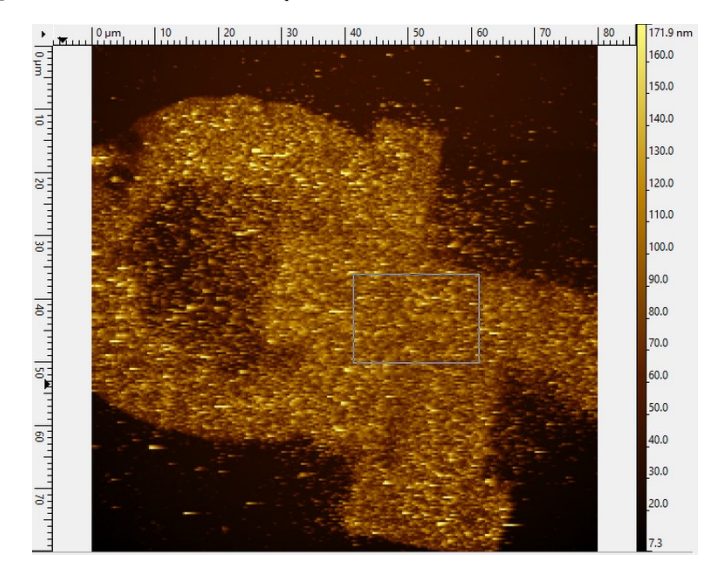


Figure S3: AFM image of the GT logo.

AFM images of the printed line features were also captured to study the effect of the laser power and the exposure time on the height of the lines. These images are shown in Fig. S4. A clear trend for the dependence of height on process parameters could not be identified with the average heights varying between 20 - 45 nm. The height measurements are summarized in Table S2.

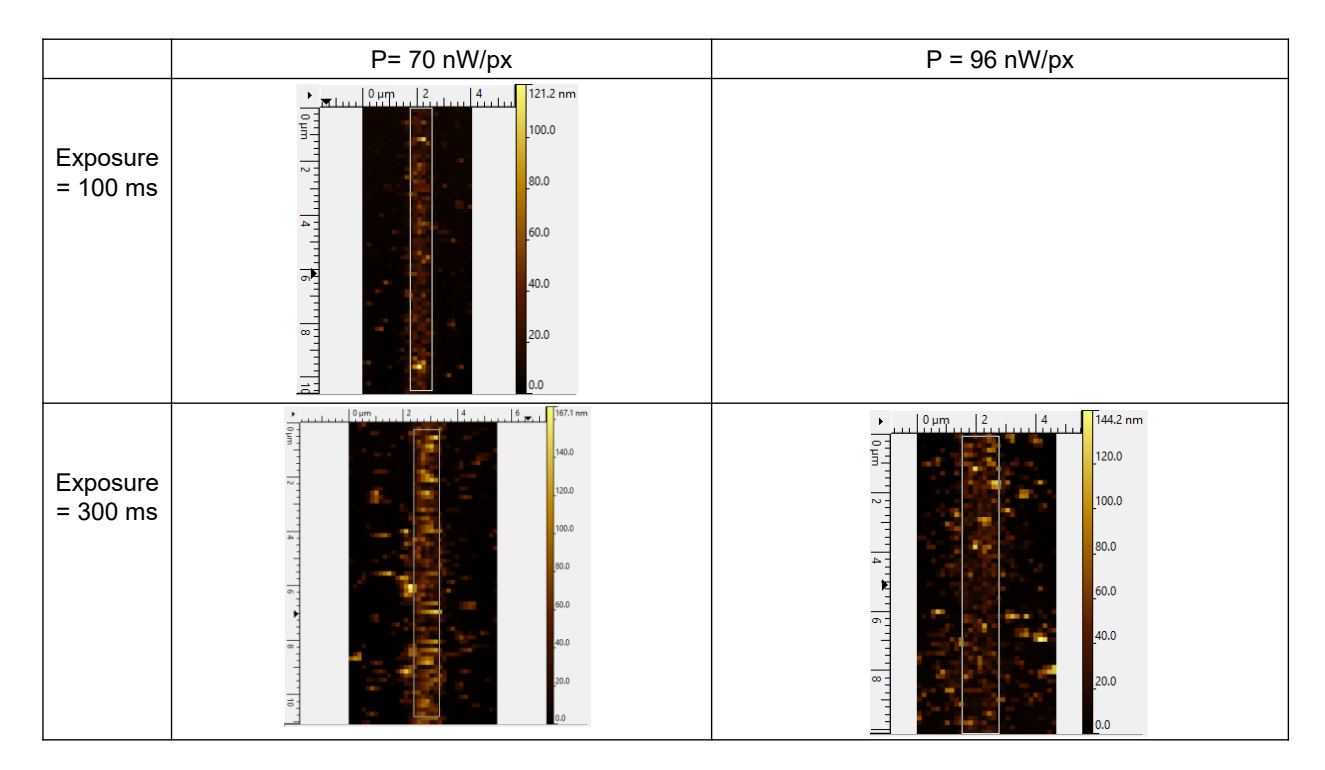


Figure S4: AFM images of the line features printed at various combinations of average powers and exposure times.

Table S2: Height of printed line features measured from AFM images

#	Process parameters	Average height (nm)	Maximum height (nm)
1	70 nW/px, 100 ms	22	121
2	70 nW/px, 300 ms	44	145
3	96 nW/px, 300 ms	23	104

S4. Conversion from average power to peak intensity

One must perform a rigorous analysis of light propagation during the temporal focusing process to accurately evaluate the peak intensity for a given average power. Instead, here we have performed a first-order approximation of the peak intensity by applying energy conservation. The total optical energy of a single pulse evaluated using the peak intensity must be the same as the pulse energy evaluated from the time-averaged power. The time-averaged power per pixel was measured at the exit of the objective lens. The pulse energy (E_p) per pixel can therefore be obtained from the time-averaged power per pixel (P) and the laser repetition rate (R) as:

$$E_{p} = \frac{P}{R} \tag{S1}$$

The pulse energy per pixel can also be obtained from the peak power per pixel (P_p) of the femtosecond pulse of duration (τ) and a Gaussian temporal shape as:

$$E_{p} = \sqrt{\frac{\pi}{2}} \tau P_{p} \tag{S2}$$

From Eqs. (S1) and (S2), the peak power can be obtained as:

$$P_{p} = \sqrt{\frac{2}{\pi}} \frac{P}{\tau R} \tag{S3}$$

The peak intensity (I_p) can then be estimated using the footprint area of each pixel (A) as:

$$I_{p} = \frac{P_{p}}{A} \tag{S4}$$

The peak intensity can be evaluated by substituting the following values for the parameters in Eqs. (S3) and (S4): P = 128 nW/pixel, $\tau = 35 \text{ fs}$, R = 5 kHz, and $A = (152 \text{ nm} \times 152 \text{ nm})/\text{pixel}$. For these parameter values, the peak intensity is 2.5 TW/cm².

S5. Conversion from average power and exposure time to laser fluence

Fluence (F) refers to the total laser energy per unit area that is incident on the exposed region. Each pulse delivers a known amount of energy per pixel (E_p) and the incident number of pulses can be evaluated from the duration of exposure (t_e) and the repetition rate of the laser (R). Therefore, the fluence can be evaluated as:

$$F = \frac{E_p R t_e}{A} \tag{S5}$$

Equation S5 can be further simplified using Eq. S1 as:

$$F = \frac{Pt_e}{A} \tag{S6}$$

For the values of P = 128 nW/pixel, $A = (152 \text{ nm} \times 152 \text{ nm})/\text{pixel}$, and $t_e = 100 \text{ ms}$, the fluence is 55 J/cm².

S6. Rate comparison of serial vs parallel TPR

The parameters and rates for this study and past studies are listed in Table S3. The areal printing rate $(A_{r,s})$ of a serial scanning two-photon reduction (TPR) process can be obtained from the scanning speed (V) and the feature width (w) as:

$$A_{r,s} = wV ag{S7}$$

For parallelization approaches that scan multiple focal spots at once, the areal rate can be evaluated by multiplying the rate for a single beam (Eq. S7) by the total number of foci. In contrast, the areal printing rate $(A_{r,p})$ of the parallel projection-TPR process can be obtained from the duration of the light exposure (t_e) and the area of projection (A_p) as:

$$A_{r,p} = \frac{A_p}{t_e} \tag{S8}$$

The areal rate was obtained directly from the values presented in the article for one of the studies (study #4 in Table S3). In that study, beam shaping was applied to generate complex structures at once.

Study Printing VAreal rate w A_p t_e modality (mm/s)(nm) (ms) (mm²/min) Tabrizi et al., 2016 (Ref 19) 0.01 200 1×10^{-4} 1 Serial scan Ishikawa et al., 2012 (Ref 20) Serial scan 0.05 400 1×10^{-3} Qian et al., 2018 (Ref 24) Multi-foci 0.01 800 3×10^{-3} scan (7 foci) Liu et al., 2019 (Ref 25) 2×10^{-3} 4 Parallel beam shaping 5 Saha et al., 2019 (Ref 26) 10 3×10^{-1} Serial scan 500 This study Parallel - $130 \times 130 \ \mu m^2$ 500 2 projection $130 \times 130 \; \mu m^2$ 7 This study Parallel -100 10 projection

Table S3: TPR printing rates for this vs past studies